Mitochondrial Fusion Mediated by Mitofusin 1 Regulates Macrophage Mycobactericidal Activity by Enhancing Autophagy

Yuping Ning,[a,b,c] Yi Cai,[a] Youchao Dai,[a] Fuxiang Li,[a,c] Siwei Mo,[a] Oliver Werz,[b] ⬤Xinchun Chen[a]

[a]Guangdong Provincial Key Laboratory of Regional Immunity and Diseases, Department of Pathogen Biology, Shenzhen University School of Medicine, Shenzhen, Guangdong, China
[b]Department of Pharmaceutical/Medicinal Chemistry, Institute of Pharmacy, Friedrich-Schiller-Universität Jena, Jena, Germany
[c]Shenzhen University-Friedrich Schiller Universität Jena Joint PhD Program, Friedrich-Schiller-Universität Jena, Jena, Germany

Yuping Ning and Yi Cai contributed equally to this work. Author order was determined by the temporal order in which the authors began performing the research.

ABSTRACT A mitochondrion, as a highly dynamic organelle, continuously changes morphology and position during its life cycle. Mitochondrial dynamics, including fission and fusion, play a critical role in maintaining functional mitochondria for ATP production, which is directly linked to host defense against *Mycobacterium tuberculosis* infection. However, how macrophages regulate mitochondrial dynamics during *M. tuberculosis* infection remains elusive. In this study, we found that *M. tuberculosis* infection induced mitochondrial fusion by enhancing the expression of mitofusin 1 (*MFN1*), which resulted in increased ATP production. Silencing of *MFN1* inhibited mitochondrial fusion and subsequently reduced ATP production, which, in turn, severely impaired macrophages' mycobactericidal activity by inhibiting autophagy. Impairment of mycobactericidal activity and autophagy was replicated using oligomycin, an inhibitor of ATP synthase. In summary, our study revealed that MFN1-mediated mitochondrial fusion is essential for macrophages' mycobactericidal activity through the regulation of ATP-dependent autophagy. The MFN1-mediated metabolism pathway might be a target for the development of a host direct therapy (HDT) strategy against tuberculosis.

KEYWORDS *Mycobacterium tuberculosis*, macrophage, mitochondrial dynamics, MFN1

Tuberculosis (TB), caused by intracellular infection by the bacterium *Mycobacterium tuberculosis*, is a leading infectious disease worldwide that killed proximately 1.4 million people in 2018 (1). Macrophages are the front-line responders to pathogens, acting as either reservoirs or killers of the bacteria (2). Immunometabolism, which supports the function and bactericidal activity of macrophages, has recently been attracting a lot of interest (3). To eliminate *M. tuberculosis* efficiently, macrophages have been reported to shift their metabolic states to glycolysis and oxidative phosphorylation (OXPHOS) to meet the bioenergetic and metabolic requirements (4).

Mitochondria are highly dynamic powerhouses that control cell energy metabolism (5). They are known to efficiently produce the bulk of the ATP needed to support cellular activities through OXPHOS and the tricarboxylic acid (TCA) cycle (6, 7). Mitochondrial dynamics, including fission and fusion, primarily regulated by mitofusins (MFNs) and dynamin-related protein 1 (DRP1), are related to the metabolic processes of OXPHOS and glycolysis (8, 9). Mitochondrial fusion increases dimerization and the activity of ATP synthase, maximizes the oxidative capacity, and maintains mitochondrial function (10).

During *M. tuberculosis* infection, biphasic immunometabolism, which involves changes in mitochondrial function, occurs in macrophages (11). However, how *M. tuberculosis* infection influences mitochondrial dynamics and the metabolic profile remains uncertain. A previous study found that different *M. tuberculosis* virulent factors altered differential

mitochondrial dynamics in macrophages (12). Jamwal et al. showed that, compared with an avirulent strain, a virulent strain of *M. tuberculosis* elongated the mitochondria and increased ATP levels in the human macrophage THP-1 cell line as a way to prevent host macrophage apoptosis (13). In contrast, Fine-Coulson et al. (14) and Lee et al. (15) found that *M. tuberculosis* induced mitochondrial fission in the human cell line A549 and a murine bone marrow-derived macrophage (BMDM) cell line, respectively.

In this study, we found that mitochondria undergo fusion during *M. tuberculosis* infection mediated by mitofusin 1 (MFN1), leading to significantly increased OXPHOS levels and ATP production. Silencing of *MFN1* inhibited mitochondrial fusion and subsequently reduced ATP production, which, in turn, severely impaired macrophages' mycobactericidal activity by inhibiting autophagy.

RESULTS

***M. tuberculosis* infection induces mitochondrial fusion in human macrophages.** To investigate the effects of *M. tuberculosis* infection on mitochondrial dynamics, we infected THP-1 macrophages with the *M. tuberculosis* strains H37Ra and H37Rv and monitored mitochondrial morphology using confocal microscopy. We found that H37Ra-infected macrophages displayed a higher rate of mitochondrial elongation and more interconnectivity of mitochondrial networks than uninfected macrophages (Fig. 1A and B; see also Fig. S1A in the supplemental material). The same phenomenon was observed with the virulent *M. tuberculosis* strain H37Rv (Fig. 1C and D). Mitochondrial fusion has been associated with increased mitochondrial membrane potential (MMP) (16, 17). We thus further investigated MMP during *M. tuberculosis* infection using MitoTraker. The MMP was significantly elevated in both H37Ra- and H37Rv-infected THP-1 macrophages at 48 h postinfection (hpi) (Fig. 1E). Additionally, compared to H37Ra, H37Rv was more robust in inducing an increase in the MMP. Increased MMP by H37Ra was further confirmed by using another MMP dye, rhodamine 123 (18). We observed a decreased intensity of rhodamine 123 staining in H37Ra-infected macrophages, indicative of increased MMP (Fig. S1B). Together, these results indicated that mitochondrial dynamics were altered by *M. tuberculosis* infection and that the mitochondria tended to form reticulate elongated fusion networks. H37Ra and H37Rv can increase MMP, and H37Rv has a stronger effect than H37Ra.

***M. tuberculosis*-induced mitochondrial fusion depends on MFN1.** Key players in the mitochondrial fusion process include the outer mitochondrial membrane GTPases mitofusin 1 (MFN1) and mitofusin 2 (MFN2) and the inner membrane GTPase optic atrophy 1 (OPA1) (19). To determine whether those proteins are involved in *M. tuberculosis*-mediated mitochondrial fusion, we analyzed the expression of these genes in *M. tuberculosis*-infected macrophages. The results show that the expression of *MFN1* significantly increased ($P < 0.0001$) in both H37Ra- and H37Rv-infected macrophages (Fig. 2A and B). The level of MFN1 protein was consistently found to be higher in the *M. tuberculosis*-infected macrophages than in the uninfected cells (Fig. 2C and D). In contrast, the levels of MFN2 and OPA1 were not significantly altered. Notably, an elevated MFN1 level was also observed in H37Ra-infected primary human monocyte-derived macrophages (hMDMs) (see Fig. S2). Considering the association between MFN1 and mitochondrial fusion, we therefore further investigated the role of MFN1 in regulating mitochondrial fusion in human macrophages induced by *M. tuberculosis* infection. To this end, we knocked down *MFN1* with small interfering RNA (siRNA) (Fig. 2E) and evaluated its effect on mitochondrial fusion. As expected, we found that silencing of *MFN1* dramatically reduced mitochondrial elongation and mitochondrial interconnectivity during H37Rv infection (Fig. 2F and G). A significant reduction in MMP in the *MFN1* knockdown macrophages was observed by using MitoTracker Red CMXRos staining (Fig. 2H). The effect of silencing *MFN1* was further confirmed by JC-1 staining using confocal microscopy (see Fig. S3). Compared to that in the si*MFN1* group, the control group showed greater red fluorescence representing JC-1 monomers, which suggests the green florescence fused with the mitochondrial matrix and formed red aggregates due to higher MMP (20).
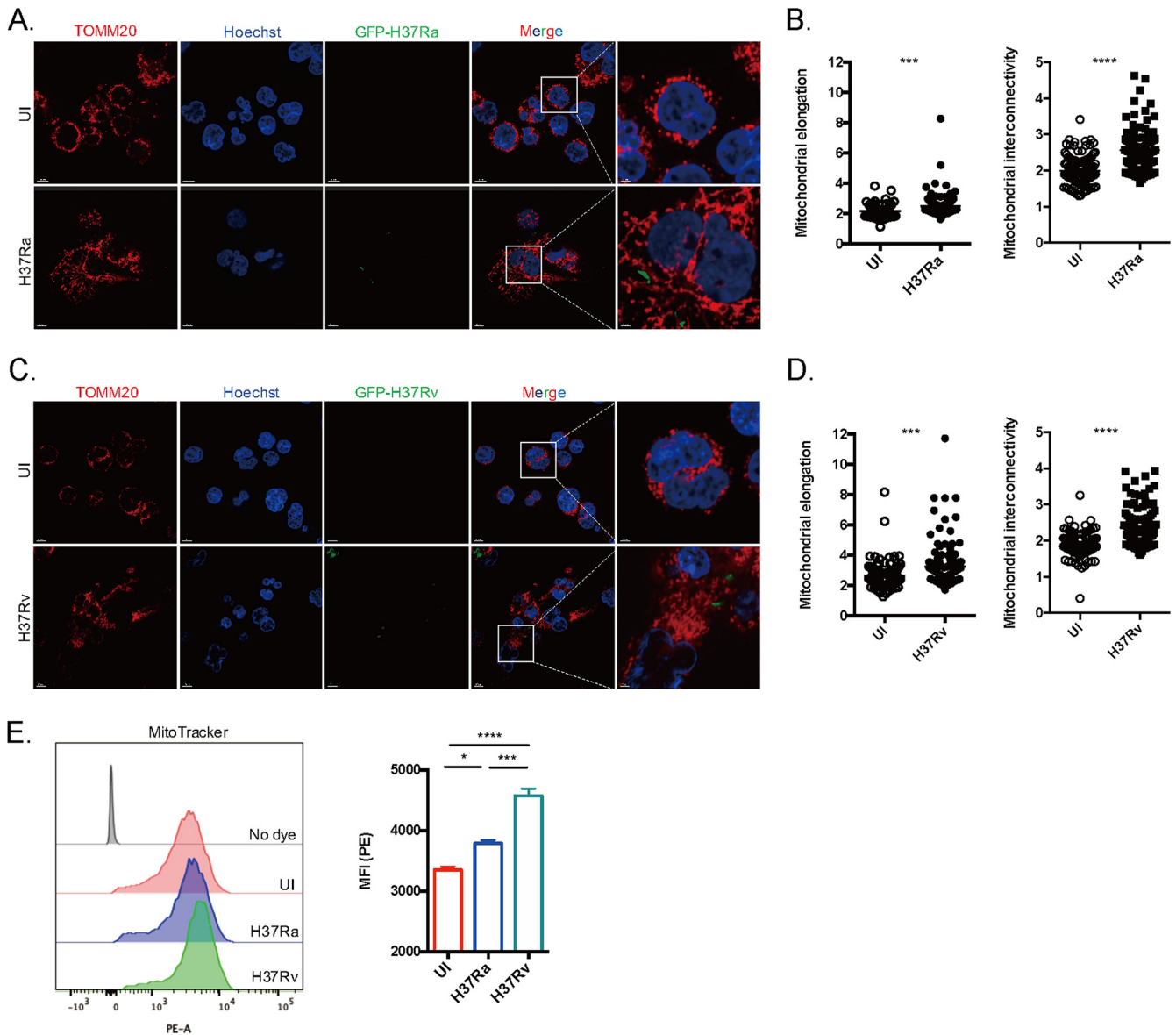
FIG 1 Mitochondrial fusion during *M. tuberculosis* infection. (A to D) Confocal microscopy images showing elongated mitochondrial morphology in THP-1 macrophages infected by H37Ra (MOI of 10:1) and H37Rv (MOI of 10:1) for 48 h. Red fluorescence, mitochondria; green fluorescence, H37Ra/Rv; blue fluorescence, Hoechst-33342-labeled nuclei. Bars, 10 μm (left) and 3 μm (right). Images (A and C) and quantitative analysis (B and D) of mitochondrial elongation and mitochondrial interconnectivity applied to the uninfected group (UI) and H37Ra/Rv-infected groups (means $\pm$ SEMs, n = 100 cells). (E) Mitochondrial membrane potential (MMP) was detected using MitoTracker Red CMXRos probes (100 nM) in H37Ra-infected (MOI of 10:1) and H37Rv-infected (MOI of 10:1) THP-1 macrophages. Mean fluorescence intensity (MFI) of MMP was analyzed by flow cytometry. Histograms indicated MFIs in the UI and H37Ra/Rv-infected groups. The data represent the means $\pm$ SEMs (n = 3). *, $P < 0.05$; ***, $P < 0.001$; ****, $P < 0.0001$.

Together, these findings indicate that *M. tuberculosis* infection induces mitochondrial fusion by increasing MFN1 expression.

Silencing of *MFN1* impairs OXPHOS and ATP production during *M. tuberculosis* infection. Increasing mitochondrial fusion indicates a heightened requirement for oxidative phosphorylation (OXPHOS) and ATP production (21). In line with this, we observed that *M. tuberculosis* infection increased ATP production and the oxygen consumption rate (OCR) (Fig. 3A and B) at 24 hpi. Given the role of MFN1 in *M. tuberculosis*-induced mitochondrial fusion, we investigated whether MFN1 expression alters the respiratory capacity during *M. tuberculosis* infection. As expected, the silencing of *MFN1* resulted in a dramatically decreased basal OCR, ATP-linked respiration, and maximum OCR in the H37Ra-infected macrophages (Fig. 3B). A decrease in ATP production was also observed in the *MFN1* knockdown macrophages during *M. tuberculosis*
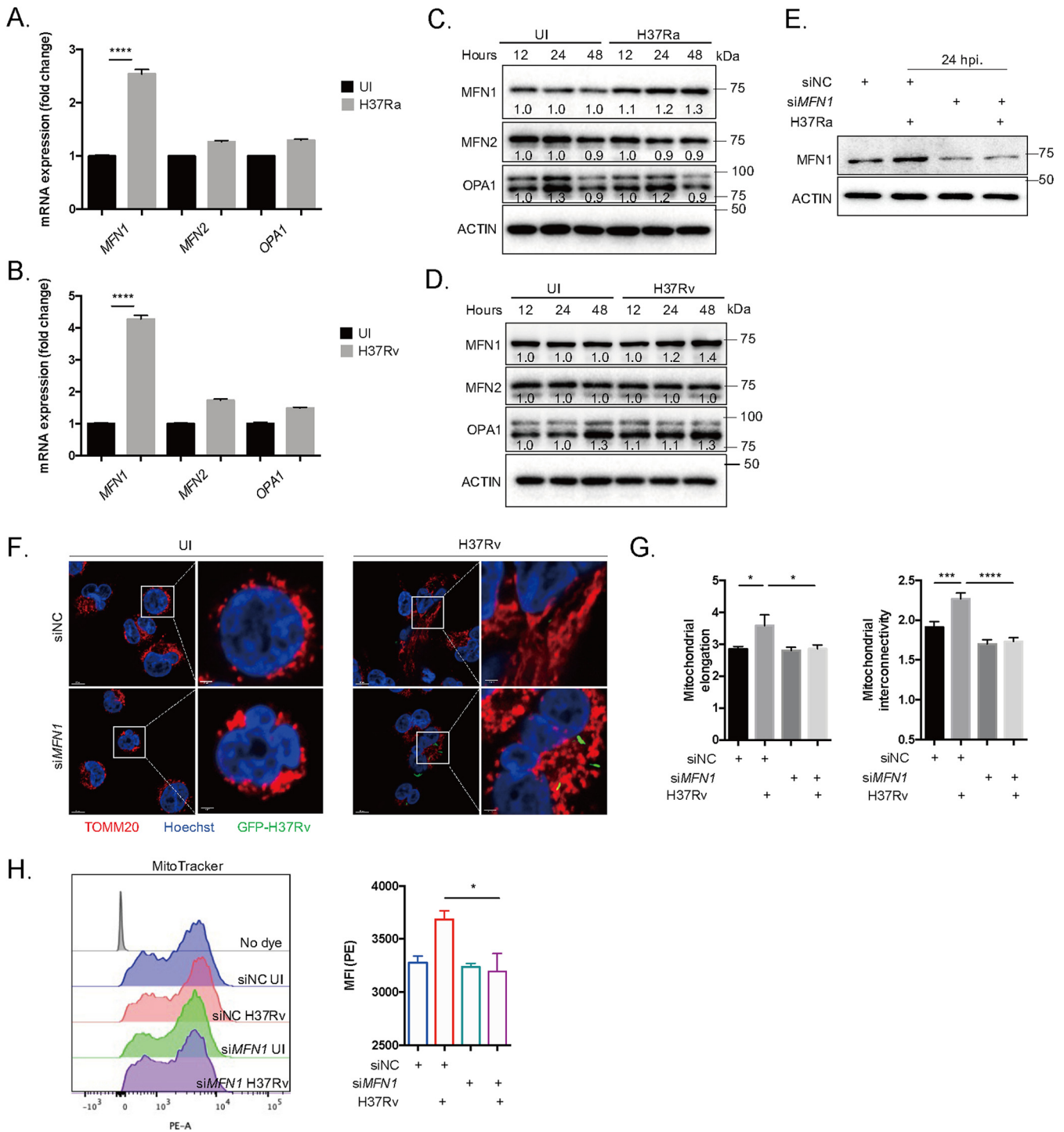
FIG 2 *M. tuberculosis*-induced mitochondrial fusion depends on MFN1. (A to D) THP-1 macrophages infected with H37Ra (MOI of 10:1) or H37Rv (MOI of 10:1). The mRNA (A and B) and protein (C and D) expression of mitochondrial fusion-related genes was analyzed by real-time-PCR and Western blotting (WB), respectively. (E)WB of siRNA-mediated *MFN1* knockdown in THP-1 macrophages. (F) Confocal microscopy images showing mitochondrial morphology in THP-1 macrophages infected by H37Rv (MOI of 10:1) for 24 h with the negative-control siRNA (siNC) or *MFN1* siRNA (si*MFN1*). Red fluorescence, mitochondria; green fluorescence, H37Ra; blue fluorescence, Hoechst 33342-labeled nuclei. Bars, 10 μm (left) and 2 μm (right). (G) Quantitative analysis of mitochondrial elongation and mitochondrial interconnectivity (means $\pm$ SEMs, $n = 30$ cells). (H) Mitochondrial membrane potential was detected using MitoTracker Red CMXRos probes (100 nM) in H37Rv-infected (MOI of 10: 1) THP-1 macrophages at 24 hpi. The data represent means $\pm$ SEMs ($n = 3$). *, $P < 0.05$; ***, $P < 0.001$; ****, $P < 0.0001$.

infection (Fig. 3C). Silencing of *MFN1* expression had almost no effect on mitochondrial reactive oxygen species (mROS) production in *M. tuberculosis*-infected and uninfected cells (see Fig. S4). In contrast, no significant changes in the extracellular acidification rate (ECAR) were found between the control group and the *MFN1* knockdown group
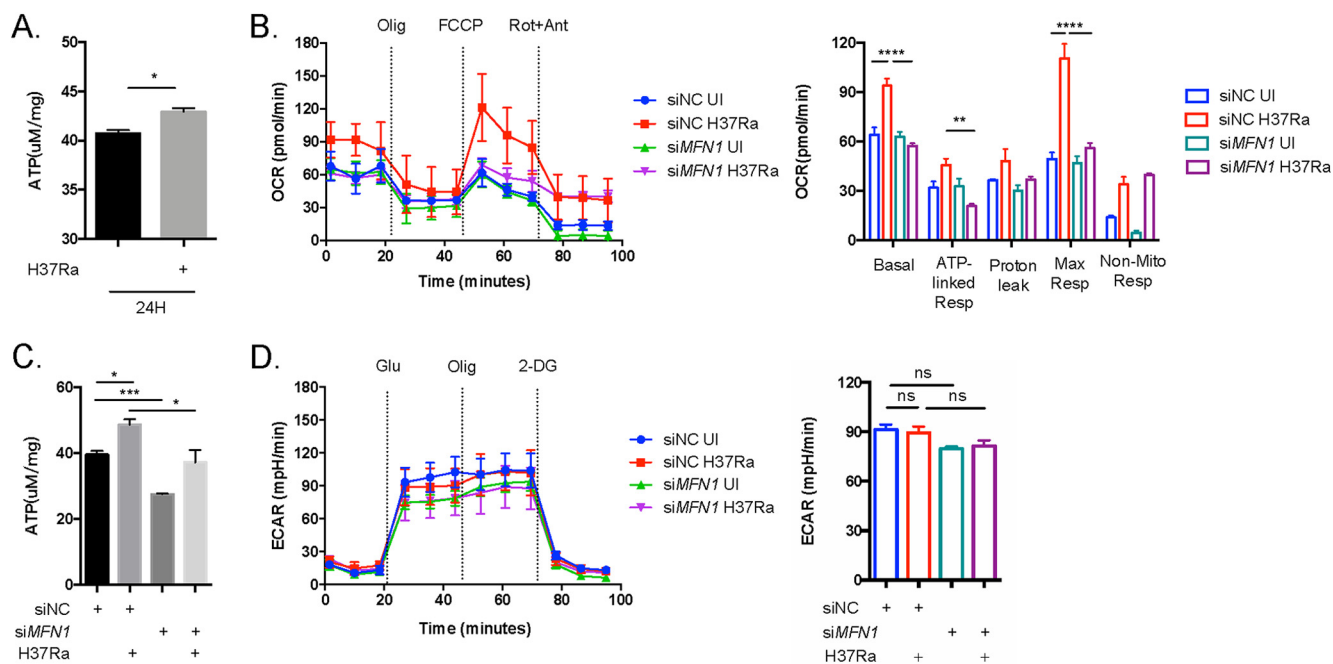
FIG 3 Silencing of *MFN1* expression impairs *M. tuberculosis*-induced OXPHOS and ATP production in THP-1 macrophages. (A) THP-1 macrophages were infected with H37Ra as indicated at an MOI of 10:1, and total intracellular ATP was measured at 24 hpi using a luminescence assay. (B) Mito Stress Test assay detected by a Seahorse XFe24 extracellular flux analyzer showing change in OCR of THP-1 macrophages after infection with H37Ra (MOI of 10:1) for 24 h. The histogram on the right shows decreased basal OCR and maximum OCR in si*MFN1* cells compared to that in negative-control siRNA (siNC) cells infected with H37Ra. (C) THP-1 macrophages were treated with siNC or si*MFN1* and then infected with H37Ra (MOI of 10:1) for 24 h; the intracellular ATP level was assessed using a luminescence assay. (D) Glycolysis stress assay showing change in ECAR of THP-1 macrophages after infection with H37Ra (MOI of 10:1) for 24 h in the presence or absence of *MFN1* siRNA. The data represent means ± SEMs ($n = 3$). *, $P < 0.05$; **, $P < 0.01$; ***, $P < 0.001$; ****, $P < 0.0001$; ns, not significant.

(Fig. 3D), suggesting that the increase in intracellular ATP production induced by *M. tuberculosis* was via OXPHOS. These results indicate that silencing of *MFN1* impairs OXPHOS and ATP production during *M. tuberculosis* infection.

MFN1 regulates macrophages' mycobactericidal activity depending on OXPHOS and ATP production. To explore whether MFN1-regulated mitochondrial fusion and respiratory capacity are linked to the host control of *M. tuberculosis* replication, we tested the effect of silencing *MFN1* on intracellular *M. tuberculosis* growth in THP-1 macrophages. We found that silencing of *MFN1* significantly enhanced both H37Ra and H37Rv growth in THP-1 macrophages at 72 hpi (Fig. 4A and B). Cells treated with si*MFN1* did not undergo significant apoptosis compared to those in the control (siNC) group (data not shown). Since si*MFN1* influences OXPHOS and ATP production, we propose that the impaired mycobactericidal activity observed in si*MFN1* macrophages is due to reduced ATP production. To test this, we applied oligomycin, an inhibitor of ATP synthase, to pharmacologically inhibit OXPHOS (22, 23) and evaluated its effect on intracellular *M. tuberculosis* growth within THP-1 macrophages. At a concentration of 10 nM, oligomycin dramatically decreased intracellular ATP in macrophages with or without H37Ra infection (Fig. 4C). When intracellular CFU numbers were recorded for the oligomycin-treated and untreated groups at 6 and 72 hpi, we confirmed that oligomycin treatment significantly impaired the THP-1 macrophages' mycobactericidal activity (Fig. 4D).

Thus, our results indicated that MFN1 expression induced by *M. tuberculosis* infection is a mechanism for host macrophages to get rid of intracellular *M. tuberculosis* by modulating mitochondrial fusion, a process with enhanced OXPHOS and ATP production.

MFN1 enhanced macrophages' bactericidal activity against *M. tuberculosis* by enhancing autophagy. Mitochondrial dynamics, including fusion and fission, are essential for modulating mitochondrial bioenergetics and a variety of cellular processes, including autophagy (24). Since autophagy is a main strategy for host defense against *M.*
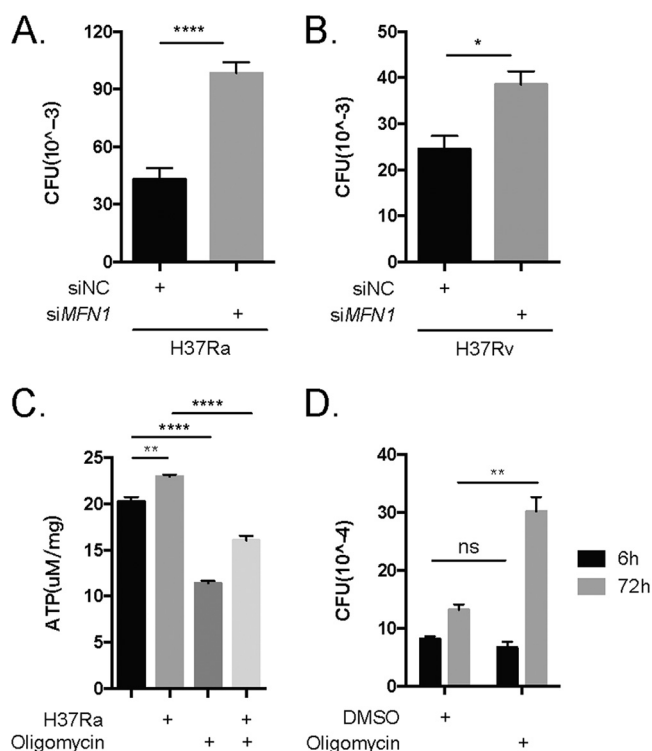
FIG 4 MFN1-mediated macrophage mycobactericidal activity depends on OXPHOS and ATP production. THP-1 macrophages were infected with H37Ra (MOI of 10:1) (A) or H37Rv (MOI of 10:1) (B) in the presence or absence of *MFN1*-siRNA and compared with those infected with negative-control siRNA (siNC) for 6 h; then, extracellular bacteria were removed and the intracellular CFU was determined at 72 hpi. (C) THP-1 macrophages treated with oligomycin (10 nM) were infected as indicated at an MOI of 10:1, and total intracellular ATP was measured at 24 hpi using a luminescence assay. (D) THP-1 macrophages treated with DMSO or oligomycin (10 μM) were infected with H37Ra (MOI of 10:1), and CFU counts were recorded at 6 hpi; for the 72-h CFU counting, extracellular bacteria were removed at 6 hpi; then, macrophage bactericidal activity was assessed by CFU counts of intracellular H37Ra at 72 hpi. The data represent means ± SEMs ($n = 3$). *, $P < 0.05$; **, $P < 0.01$; ****, $P < 0.0001$; ns, not significant.

tuberculosis, we first investigated the effect of MFN1 on autophagy induction during *M. tuberculosis* infection. We found that silencing of *MFN1* significantly inhibited autophagy in H37Rv-infected macrophages, as evidenced by a significant decrease in LC3B-II (Fig. 5A). si*MFN1* also impaired H37Ra-induced LC3B-II expression (see Fig. S5A). Second, we used autophagosome-lysosome fusion inhibitors, chloroquine and bafilomycin A1, which lead to LC3B-II accumulation and a higher level of LC3B-II (25), to confirm whether the reduced LC3B-II signal in the si*MFN1* group was caused by inhibition of autophagy flux rather than an acceleration of it. We found a significantly decreased LC3B-II level in the si*MFN1* group compared to that in control macrophages both treated with chloroquine and bafilomycin A1 (Fig. S5B), indicating si*MFN1* inhibits the initiation of the autophagy process rather than the acidification of autophagosomes. To confirm that knockdown of *MFN1* limits antimicrobial autophagy, we analyzed the colocalization of p62/LC3B with green fluorescent protein (GFP)-H37Ra (see Fig. S6). We found that si*MFN1* significantly decreased the colocalization of LC3/p62 and GFP-H37Ra compared to that in the siNC group.

Consistent with the role of ATP we proposed for MFN-mediated mycobactericidal activity, we found that inhibition of mitochondrial respiration by oligomycin significantly reduced the level of LC3B-II in both H37Ra- and H37Rv-infected macrophages (Fig. 5B and Fig. S5C). The link between the inhibition of cellular ATP production and autophagy was further confirmed by inhibitors of the electron transport chain (Fig. S5D and E).
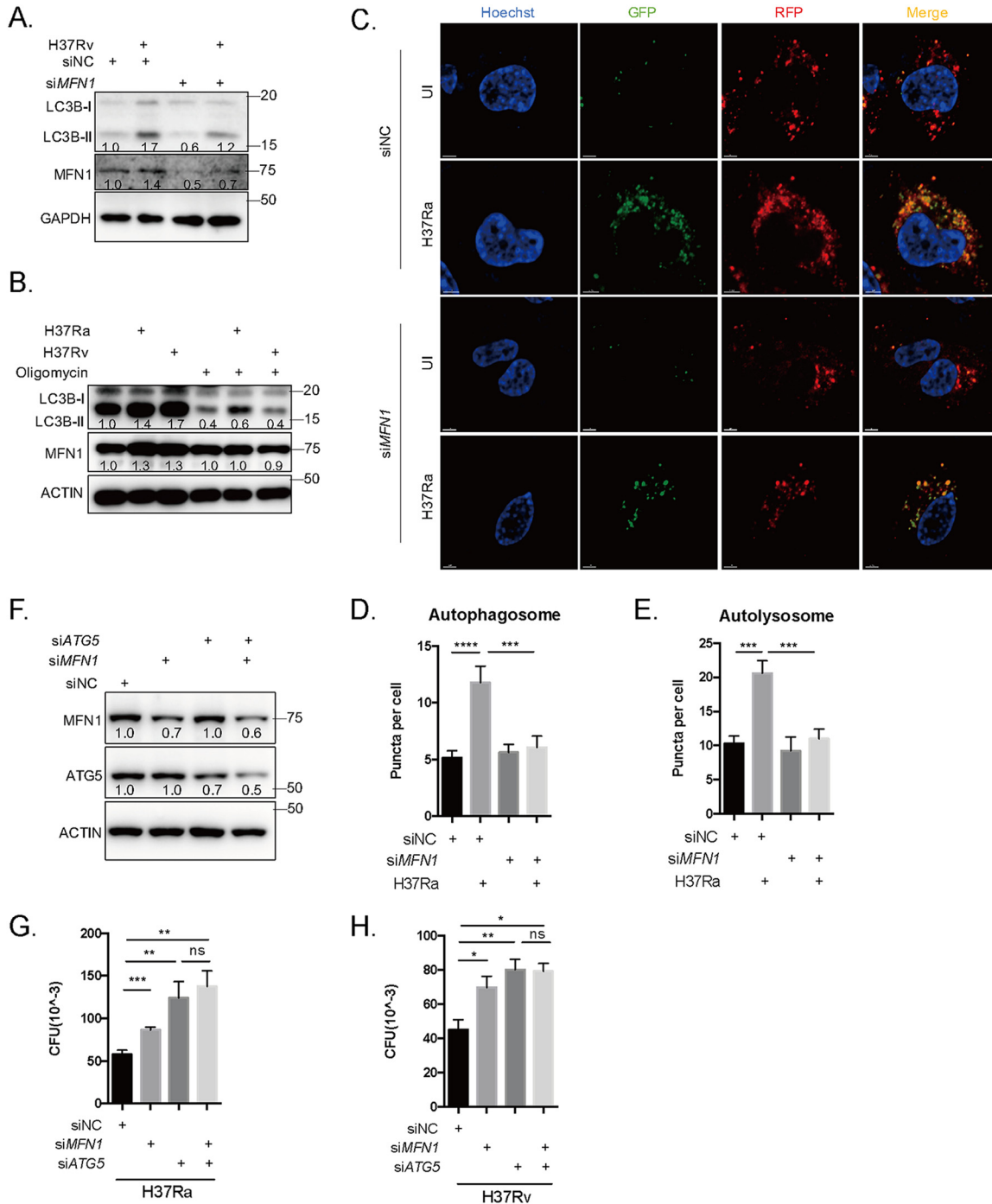
FIG 5 MFN1 mediated intracellular *M. tuberculosis* elimination by enhancing autophagy. Cell lysates were harvested from UI and 48-h H37Rv-infected (MOI of 10:1) THP-1 macrophages treated with or without *MFN1* siRNA and compared with those infected with negative-control siRNA (siNC) (A) and 24-h H37Ra/H37Rv-infected THP-1 macrophages treated with or without oligomycin (B). For Western blot analysis of MFN1 and LC3B-II expression, β-actin was used as the loading control. Confocal microscopy images (C) and histograms (D and E) ($n = 30$ to 40 cells) showing autophagy flux in mRFP-GFP-LC3 reporter THP-1 macrophages infected by H37Ra (MOI of 10:1) for 24 h with siNC and si*MFN1* treatment. Bars, 5 μm. When the autophagosome newly forms, both RFP- and GFP-LC3-II exist, showing yellow florescence; when the autophagosome fuses with a lysosome, GFP is diminished, showing red florescence, indicating the formation of the autolysosome. (F) Cell lysates were harvested from UI and 24-h H37Ra-infected (MOI of 10:1) THP-1 macrophages treated with *ATG5* siRNA and *MFN1* siRNA. For Western blot analysis of ATG5 and MFN1, β-actin was used as the loading control. THP-1 macrophages treated with or without *MFN1* and *ATG5* siRNA were infected with H37Ra (MOI of 10:1) (G) and H37Rv (MOI of 10:1) (H) for 6 h, and then extracellular bacteria were removed and intracellular CFU number was determined at 72 hpi. The data represent means ± SEMs ($n = 3$). *, $P < 0.05$; **, $P < 0.01$; ***, $P < 0.001$; ****, $P < 0.0001$; ns, not significant.

We then used a stably transformed the monomeric red fluorescent protein (mRFP)-GFP-LC3 reporter into THP-1 macrophages (26) to further determine the effect of MFN1 on autophagy flux. Silencing of *MFN1* significantly reduced the numbers of autophagosomes and autolysosomes, which formed puncta structures in H37Ra-infected macrophages (Fig. 5C to E), indicating that MFN1 is necessary for autophagy during *M. tuberculosis* infection.

Last, we confirm the role of autophagy in MFN1-mediated suppression of intracellular *M. tuberculosis* growth. To this end, we knocked down *ATG5*, which encodes a key protein for autophagy initiation and processing (27), and analyzed its effect on MFN1-mediated macrophage bactericidal activity. ATG5 expression was significantly reduced following treatment with *ATG5*-specific siRNA for 48 h (Fig. 5F). As expected, when ATG5 was intact, silencing of *MFN1* lead to higher CFU numbers of both intracellular H37Ra and H37Rv. However, when *ATG5* was knocked down, the effects of si*MFN1* on intracellular H37Ra and H37Rv replication were no longer observed (Fig. 5G and H). Together, these results demonstrated that MFN1 enhanced intracellular *M. tuberculosis* survival by reducing autophagy.

DISCUSSION

The production of adequate energy is essential to fit the immunometabolic demand by macrophages to fight against *M. tuberculosis* infection (28). In this study, we demonstrated that the mitochondrial fusion events that take place in *M. tuberculosis*-infected human THP-1 macrophages are regulated for host defense against *M. tuberculosis*. We first found that *M. tuberculosis* infection-induced expression of MFN1, a GTPase located on the mitochondrial outer membrane, has a vital role in mitochondrial fusion. MFN1-mediated mitochondrial fusion enhances OXPHOS and ATP production. This role of MFN1 is linked to macrophage bactericidal activity, which is attributed to the modulation of autophagy via mitochondrial OXPHOS and ATP production.

The importance of mitochondrial dynamics during *M. tuberculosis* infection was recently recognized (12–15). However, its role in bactericidal activity and the underlying mechanism remain uncertain. For example, Lee et al. reported that mitochondria in murine macrophages undergo fission, involving the degradation of MFN2, during H37Ra and H37Rv infections (15). This dynamic change causing apoptosis is attributable to the defensive processes of the host cell (15). In line with this report, we also found that MFN2 is decreased in Raw 264.7 murine macrophages (see Fig. S2 in the supplemental material). However, a similar result was not observed in human macrophages in our study, suggesting a difference in mitochondrial dynamics between humans and mice. Indeed, as reported by Vijayan et al., human macrophages rely more heavily on OXPHOS than glycolysis for ATP production when stimulated with lipopolysaccharide (LPS), which completely contrasts that in murine macrophages (29). Contradictory results were also found in human macrophages (30). Chen et al. (30) found that H37Rv, but not H37Ra, transiently depleted $DiOC_6(3)$ (which indicates mitochondrial inner membrane potential). At 12 and 24 hpi, the number of macrophages with depleted mitochondrial $DiOC_6(3)$ returned almost to baseline with both H37Ra and H37Rv infection, which indicates the macrophages had the ability to recover mitochondrial function after infection. Furthermore, although $DiOC_6(3)$ was used as a classical fluorescence dye for MMP (31), this probe can bind other organelles in addition to mitochondria, such as the endoplasmic reticulum (32, 33). It is not unexpected that $DiOC_6(3)$ has high sensitivity to plasma membrane depolarization (34). So, $DiOC_6(3)$ is more reliable for estimations of plasma membrane potential (PMP) than for mitochondrial membrane potential (34).

MFN2, a homolog of MFN1, plays an important role in the innate immunity against *M. tuberculosis* (15, 35–37). Recently, Tur et al. found that MFN2 has an important function in maintaining the autophagy process in BMDMs, whereas, in the absence of MFN2, autophagosome accumulation is dramatically diminished (36). Lloberas et al. further suggested that decreased ROS release in the absence of MFN2 contributes to

impaired autophagy and apoptosis (37). This suggests there is a strong association between mitochondrial dynamics and autophagy. Despite the high homology between MFN2 and MFN1, MFN1 has distinct functions and shows a higher affinity for GTP (36), which means that MFN1 has greater activity to regulate mitochondrial fusion and metabolism reprogramming (21). During metabolism reprogramming, MFN1 shifts the cellular metabolism from aerobic glycolysis to OXPHOS (38), leading to higher ATP production (21). To our knowledge, our report is the first to link the function of MFN1 as a newly innate immune modulator.

In general, autophagy is initiated to recover ATP levels and avoid cell death when cellular energy is limited, such as during an increased AMP/ATP ratio or during amino acid starvation (39). However, cellular ATP levels are also fundamental for autophagy initiation and are required in several steps during autophagy (40, 41). Mitochondrial fusion maximizes OXPHOS (42) and increases ATP production (43), which is important for supplying the immune cell's metabolic and other energy-dependent processes (44). Moreover, a mitochondrial respiratory deficiency and loss of MMP have also been reported to inhibit autophagy by upregulating protein kinase A (PKA) activity (45), a phenomenon with which our results seem to concur. Thus, we support the hypothesis that mitochondrial respiratory capacity and ATP production contribute to autophagy against *M. tuberculosis*.

In conclusion, we first discovered that MFN1-mediated mitochondrial fusion in human THP-1 macrophages is a defensive strategy against *M. tuberculosis*. Mitochondrial fusion leads to an increase in mitochondrial OXPHOS and intracellular ATP production, which fuels the autophagy process to inhibit the intracellular growth of *M. tuberculosis*. Therefore, host-directed therapy targeting mitochondrial dynamics and metabolism reprogramming might become a potential candidate for *M. tuberculosis* treatment research.

MATERIALS AND METHODS

***M. tuberculosis* culture and infection.** *M. tuberculosis* H37Ra and H37Rv strains were cultured in 7H9 broth (BD Biosciences, San Jose, CA, USA) supplemented with 10% Middlebrook oleic acid-albumin-dextrose-catalase (OADC) enrichment (BBL) containing 0.05% Tween 80 (Sigma-Aldrich) and 0.2% glycerol (Sigma-Aldrich, Merck, Darmstadt, Germany) for 1 to 2 weeks at 37°C with shaking to the mid-logarithmic phase (optical density at 600 nm [OD_{600}] of 0.3 to 0.8) prior to experiments. In all experiments involving mycobacterial infection, THP-1 macrophages were infected with *M. tuberculosis* H37Ra or H37Rv at a multiplicity of infection (MOI) of 10 mycobacteria to 1 macrophage. Before infection, the 7H9-cultured bacteria were washed once with phosphate-buffered saline (PBS), resuspended in serum-free RPMI 1640 medium, and then sonicated for 5 min to obtain a single-cell suspension. The *M. tuberculosis* cells were not opsonized before infection.

Cell culture, macrophage differentiation, and drug treatments. The human monocytic cell line THP-1 (ATCC) and THP-1 macrophages which were transformed with an mRFP-GFP-LC3B reporter (kindly provided by Hongbo Shen, Institute Pasteur of Shanghai, Shanghai, China) (26) were cultured in RPMI 1640 medium (Corning, NY, USA) supplemented with 10% (vol/vol) calf serum (Gibco, Thermo Fisher, Waltham, MA, USA) and differentiated at 37°C in 5% CO_2 using 20 ng/ml phorbol 12-myristate 13-acetate (PMA) (P8139; Sigma) for 24 h. The murine macrophage cell line Raw 264.7 (ATCC) was cultured in Dulbecco's modified Eagle medium (DMEM; Corning) supplemented with 10% (vol/vol) calf serum (Gibco, Thermo Fisher) as well. Fresh preheated culture medium was added before an overnight resting period.

Peripheral blood mononuclear cells (PBMCs) were isolated from healthy donated whole blood using Lymphoprep (07851; Stemcell, Canada) and then centrifuged at 2000 rpm for 20 min. Isolated PBMCs were washed with PBS, resuspended in RPMI 1640 medium supplemented with 50 ng/ml recombinant human macrophage colony-stimulating factor (M-CSF) (AF-300-25-500; PeproTech, Cranbury, NJ, USA), and then cultured at 37°C in 5% CO_2 for 5 days for differentiation into human monocyte-derived macrophages (hMDMs) before infection.

Bafilomycin A (HY-100558; MCE, Monmouth Junction, NJ, USA) was diluted in dimethyl sulfoxide (DMSO; Sigma-Aldrich, Merck) to a 100 μM stock solution and diluted to a 20 nM working solution. Chloroquine (HY-17589A; MCE) was diluted in DMSO to a 50 mM stock solution and diluted to a 5 μM working solution. Electron transport chain (ETC) inhibitors, including oligomycin (HY-N6782; MCE), were diluted in DMSO to a 10 μM stock solution and diluted to a 10 nM working solution. Piericidin A (MZ9233; Maokangbio, Shanghai, China) was diluted in DMSO to a 1 mM stock solution and diluted to a 10 nM working solution. Rotenone (HY-B1756; MCE) was diluted in DMSO to a 1 mM stock solution and diluted to a 1 μM working solution. Antimycin A (MS0070; Maokangbio) was diluted in DMSO to a 2.5-mg/ml stock solution and diluted to a 100 nM working solution.

Human samples. The use of all human samples used in the present study was approved by the Institutional Review Board of the Shenzhen University School of Medicine, China, and informed written consent was obtained from each participant.

RNA interference. THP-1 macrophages were seeded at a density of 4×10^5 cells per well into 12-well culture plates. After a 24-h PMA differentiation, the THP-1 macrophages were transfected with *MFN1* siRNA (RiboBio, Guangzhou, China), and scrambled siRNA (RiboBio) was used as a negative control. The sequence of siRNA targeting *MFN1* is 5′-GCACACTATCAGAGCTAAA-3′. Transfection was performed by using Lipofectamine RNAiMAX (Thermo Fisher) according to the manufacturer's protocol. Fresh medium was added after a 6-h transfection, and then the cells were rested for 48 h.

RNA preparation, reverse transcription-PCR, and real-time PCR. Total cellular RNA was extracted using a total RNA kit (R6634-02; Omega Bio-tek, Norcross, GA, USA), and the isolated RNA was reverse transcribed into cDNA with HiScript II Q RT supermix (R223-01; Vazyme, Nanjing, China) according to the manufacturer's instructions. The cDNA was mixed with 2× SYBR green quantitative PCR (qPCR) master mix (B21202; Bimake, Houston, TX, USA), and the real-time PCR was performed on a 7500 real-time PCR system (ABI, Thermo Fisher). The primers used for the real-time PCR are listed in Table S1 in the supplemental material.

Western blot analysis. Differentiated THP-1 macrophages, which were transfected with siRNA and infected with *M. tuberculosis* for 24 and 48 h, were lysed in SDS lysis buffer and subjected to Western blotting (WB). The protein samples were loaded and separated using 10% or 15% sodium dodecyl sulfate-polyacrylamide gel electrophoresis (SDS-PAGE) and then transferred onto a polyvinylidene difluoride membrane (Immobilon-P). The membrane was then blocked with 5% bovine serum albumin (BSA) in 0.1% Tween 20-PBS at room temperature for 2 h and incubated with primary antibody at 4°C overnight. Blots were visualized on Minichemi chemiluminescence imaging system (SageCreation, Beijing, China) by adding SuperSignal West Pico PLUS chemiluminescence substrate (Thermo Fisher). The primary antibodies were rabbit monoclonal anti-MFN1 (1:1,000, D6E2S; CST, Danvers, MA, USA), rabbit polyclonal anti-MFN1 (1:1,000, A9880; ABclonal, Woburn, MA, USA), rabbit monoclonal anti-MFN2 (1:1000, A19678; ABclonal), rabbit polyclonal anti-OPA1 (1:1,000, A9833; ABclonal); rabbit polyclonal anti-DRP1 (1:1,000, A16661; ABclonal), anti-actin (1:5,000, ab179467; Abcam, Cambridge, UK), rabbit monoclonal anti-LC3B (1:1,000, A19665; ABclonal), and rabbit monoclonal anti-ATG5 (1:1,000, D5F5U; CST). The secondary antibodies were goat polyclonal anti-rabbit IgG (conjugated to horseradish peroxidase [HRP]) (1:5,000, ab6721; Abcam) and goat polyclonal anti-mouse IgG HRP (1:5,000, ab6789; Abcam).

CFU assay. For the CFU count, 5×10^5 differentiated THP-1 macrophages were seeded into each well of a 12-well plate and infected with mycobacteria, as described previously. After 6 h of infection, extracellular bacteria were removed by washing twice with sterile PBS. Fresh preheated culture medium was added, and the cells were rested for 72 h. Extracellular bacteria were removed by washing twice with sterile PBS. The cells were lysed in 0.1% SDS gradient dilution in sterile PBS and then plated onto 7H10 agar plates. The plates were incubated at 37°C with 5% CO_2 for 2 to 3 weeks, and the colonies were enumerated.

Immunofluorescence and mitochondrial morphology analysis. Differentiated THP-1 macrophages were grown on 35-mm coverslips at a low density (2×10^5 per well), followed by transfection with siRNA and infection with H37Ra/H37Rv for 24 to 48 h. The cells were fixed for 15 min in 4% paraformaldehyde (Biosharp, South Jordan, UT, USA) at 37°C, permeabilized for 10 min in 0.03% Triton X-100, and blocked for 30 min with 3% BSA in 0.1% Tween 20-PBS. The cells were incubated with mouse monoclonal anti-TOMM20 antibody (1:1,000, ab56783; Abcam), rabbit monoclonal anti-LC3B (1:500, A19665; ABclonal), or mouse monoclonal anti-p62 antibody (1:500, sc-28359; Santa Cruz Biotecnology) overnight at 4°C. On the second day, the cells were equilibrated to room temperature for 1 h, washed with PBS, incubated for 1 h with secondary antibody Alexa Fluor 555 goat anti-mouse IgG(H+L) (A21422; Thermo Fisher), washed with PBS, incubated with Hoechst 33342, washed with PBS, and treated with antifade solution. The cells were visualized under a 60× oil immersion lens objective on a confocal microscope (Nikon A1R).

Mitochondrial morphology was analyzed by ImageJ software. The ImageJ macro was downloaded from ImageJ Documentation Wiki (http://imagejdocu.tudor.lu/plugin/morphology/mitochondrial_morphology _macro_plug-in/start). This method was validated previously (46). The mean area/perimeter ratio was employed as an index of mitochondrial interconnectivity, with inverse circularity used as a measure of mitochondrial elongation, as validated using well-characterized mediators of mitochondrial fission and fusion. Scoring was performed in a blinded manner.

MMP assays, mROS assays, and flow cytometry. For analysis of MMP, differentiated THP-1 macrophages were infected with H37Ra/Rv for 48 h. Before staining, cells were washed with PBS. Infected and uninfected THP-1 macrophages were then stained with 100 nM MitoTracker Red CMXRos (M7512; Thermo Fisher) or 1 μM rhodamine 123 (C2007; Beyotime) in culture medium for 30 min at 37°C. After washing twice with PBS, the cells were processed for flow cytometry. For the JC-1 assay, THP-1 macrophages were prepared as mentioned above, and a JC-1 assay kit (C2006; Beyotime, Shanghai, China) was used according to the manufacturer's instructions. For analysis of the mROS release level, infected or uninfected THP-1 macrophages were stained with 10 μM MitoSOX Red mitochondrial superoxide indicator (M36008; Invitrogen, Thermo Fisher). Flow cytometry was carried on BD FACSAriaII cell sorter (BD biosciences), and analysis was performed using FlowJo software.

ATP assay. For the ATP assay, differentiated THP-1 macrophages transfected with si*MFN1* siRNA or treated with oligomycin were infected with H37Ra for 24 h. The intracellular ATP levels of THP-1 macrophages were evaluated using the Enhanced ATP assay kit (S0027; Beyotime) according to the manufacturer's instructions.

OCR assay. The OCR and ECAR of THP-1 macrophages were determined using the Seahorse XFe24 extracellular flux analyzer (Agilent Technologies, Santa Clara, CA, USA). Cells were seeded at 8×10^4 per well, differentiated with PMA for 24 h, and then transfected with scramble siRNA or si*MFN1* siRNA as previously described. THP-1 macrophages were infected with H37Ra for 24 h. We used the Seahorse XF Cell Mito Stress Test kit (103015-100; Seahorse Bioscience) for the OCR assay. Electron transport chain inhibitors were added every 20 min from the beginning in the following order: oligomycin (1.5 μM), 2-{2-[4-(trifluoromethoxy)phenyl]hydrazinylidene}-propanedinitrile (FCCP; 1 μM), and then a combination of rotenone (0.5 μM) and antimycin A (0.5 μM). For the ECAR assay, the Seahorse XF Glycolysis Stress Test kit (103020-100; Seahorse Bioscience) was used. All readings were normalized to the protein level of each well using a bicinchoninic acid (BCA) protein assay kit (P0011; Beyotime).

Statistical analysis. Statistical analysis was performed using GraphPad Prism 6 software (GraphPad Software, Inc.). A two-tailed unpaired Student's *t* test was used to evaluate the significance of single parameters between two groups. One-way analysis of variance (ANOVA) with multiple comparisons was used to analyze more than two groups. Data are expressed as means ± standard errors of the means (SEMs) ($n = 3$).

SUPPLEMENTAL MATERIAL

Supplemental material is available online only.

SUPPLEMENTAL FILE 1, PDF file, 0.9 MB.
SUPPLEMENTAL FILE 2, PDF file, 0.2 MB.
SUPPLEMENTAL FILE 3, PDF file, 1.3 MB.
SUPPLEMENTAL FILE 4, PDF file, 0.4 MB.
SUPPLEMENTAL FILE 5, PDF file, 2.1 MB.
SUPPLEMENTAL FILE 6, PDF file, 1.1 MB.
SUPPLEMENTAL FILE 7, PDF file, 0.1 MB.
SUPPLEMENTAL FILE 8, PDF file, 0.1 MB.

REFERENCES

1. World Health Organization. 2019. Global tuberculosis report. World Health Organization, Geneva, Switzerland.
2. Howard NC, Khader SA. 2020. Immunometabolism during *Mycobacterium tuberculosis* infection. Trends Microbiol 28:832–850. https://doi.org/10.1016/j.tim.2020.04.010.
3. Cumming BM, Pacl HT, Steyn AJC. 2020. Relevance of the Warburg effect in tuberculosis for host-directed therapy. Front Cell Infect Microbiol 10:576596. https://doi.org/10.3389/fcimb.2020.576596.
4. Angajala A, Lim S, Phillips JB, Kim J-H, Yates C, You Z, Tan M. 2018. Diverse roles of mitochondria in immune responses: novel insights into immuno-metabolism. Front Immunol 9:1605. https://doi.org/10.3389/fimmu.2018.01605.
5. Vyas S, Zaganjor E, Haigis MC. 2016. Mitochondria and cancer. Cell 166:555–566. https://doi.org/10.1016/j.cell.2016.07.002.
6. Nazaret C, Heiske M, Thurley K, Mazat JP. 2009. Mitochondrial energetic metabolism: a simplified model of TCA cycle with ATP production. J Theor Biol 258:455–464. https://doi.org/10.1016/j.jtbi.2008.09.037.
7. Benmoussa K, Garaude J, Acin-Perez R. 2018. How mitochondrial metabolism contributes to macrophage phenotype and functions. J Mol Biol 430:3906–3921. https://doi.org/10.1016/j.jmb.2018.07.003.
8. Cloonan SM, Choi AM. 2016. Mitochondria in lung disease. J Clin Invest 126:809–820. https://doi.org/10.1172/JCI81113.
9. Son MJ, Kwon Y, Son MY, Seol B, Choi HS, Ryu SW, Choi C, Cho YS. 2015. Mitofusins deficiency elicits mitochondrial metabolic reprogramming to pluripotency. Cell Death Differ 22:1957–1969. https://doi.org/10.1038/cdd.2015.43.
10. Gomes LC, Di Benedetto G, Scorrano L. 2011. During autophagy mitochondria elongate, are spared from degradation and sustain cell viability. Nat Cell Biol 13:589–598. https://doi.org/10.1038/ncb2220.
11. Shi LB, Jiang QK, Bushkin Y, Subbian S, Tyagi S. 2019. Biphasic dynamics of macrophage immunometabolism during *Mycobacterium tuberculosis* infection. mBio 10:e02550-18. https://doi.org/10.1128/mBio.02550-18.
12. Aguilar-Lopez BA, Correa F, Moreno-Altamirano MMB, Espitia C, Hernandez-Longoria R, Oliva-Ramirez J, Padierna-Olivos J, Sanchez-Garcia FJ. 2019. LprG and PE_PGRS33 *Mycobacterium tuberculosis* virulence factors induce differential mitochondrial dynamics in macrophages. Scand J Immunol 89:e12728. https://doi.org/10.1111/sji.12728.
13. Jamwal S, Midha MK, Verma HN, Basu A, Rao KV, Manivel V. 2013. Characterizing virulence-specific perturbations in the mitochondrial function of macrophages infected with *Mycobacterium tuberculosis*. Sci Rep 3:1328. https://doi.org/10.1038/srep01328.
14. Fine-Coulson K, Giguere S, Quinn FD, Reaves BJ. 2015. Infection of A549 human type II epithelial cells with *Mycobacterium tuberculosis* induces changes in mitochondrial morphology, distribution and mass that are dependent on the early secreted antigen, ESAT-6. Microbes Infect 17:689–697. https://doi.org/10.1016/j.micinf.2015.06.003.
15. Lee J, Choi JA, Cho SN, Son SH, Song CH. 2019. Mitofusin 2-deficiency suppresses *Mycobacterium tuberculosis* survival in macrophages. Cells 8:1355. https://doi.org/10.3390/cells8111355.

16. Zorova LD, Popkov VA, Plotnikov EY, Silachev DN, Pevzner IB, Jankauskas SS, Babenko VA, Zorov SD, Balakireva AV, Juhaszova M, Sollott SJ, Zorov DB. 2018. Mitochondrial membrane potential. Anal Biochem 552:50–59. https://doi.org/10.1016/j.ab.2017.07.009.

17. Yoshizumi T, Ichinohe T, Sasaki O, Otera H, Kawabata S, Mihara K, Koshiba T. 2014. Influenza A virus protein PB1-F2 translocates into mitochondria via Tom40 channels and impairs innate immunity. Nat Commun 5:4713. https://doi.org/10.1038/ncomms5713.

18. Baracca A, Sgarbi G, Solaini G, Lenaz G. 2003. Rhodamine 123 as a probe of mitochondrial membrane potential: evaluation of proton flux through Fo during ATP synthesis. Biochim Biophys Acta 1606:137–146. https://doi.org/10.1016/S0005-2728(03)00110-5.

19. Pyakurel A, Savoia C, Hess D, Scorrano L. 2015. Extracellular regulated kinase phosphorylates mitofusin 1 to control mitochondrial morphology and apoptosis. Mol Cell 58:244–254. https://doi.org/10.1016/j.molcel.2015.02.021.

20. Sivandzade F, Bhalerao A, Cucullo L. 2019. Analysis of the mitochondrial membrane potential using the cationic JC-1 dye as a sensitive fluorescent probe. Bio Protoc 9:e3128. https://doi.org/10.21769/BioProtoc.3128.

21. Son JM, Sarsour EH, Kakkerla Balaraju A, Fussell J, Kalen AL, Wagner BA, Buettner GR, Goswami PC. 2017. Mitofusin 1 and optic atrophy 1 shift metabolism to mitochondrial respiration during aging. Aging Cell 16:1136–1145. https://doi.org/10.1111/acel.12649.

22. Steinmetz J, Senkowski W, Lengqvist J, Rubin J, Ossipova E, Herman S, Larsson R, Jakobsson PJ, Fryknas M, Kultima K. 2020. Descriptive proteome analysis to investigate context-dependent treatment responses to OXPHOS inhibition in colon carcinoma cells grown as monolayer and multicellular tumor spheroids. ACS Omega 5:17242–17254. https://doi.org/10.1021/acsomega.0c01419.

23. Zhang Y, Nguyen TTT, Shang E, Mela A, Humala N, Mahajan A, Zhao J, Shu C, Torrini C, Sanchez-Quintero MJ, Kleiner G, Bianchetti E, Westhoff MA, Quinzii CM, Karpel-Massler G, Bruce JN, Canoll P, Siegelin MD. 2020. MET inhibition elicits PGC1alpha-dependent metabolic reprogramming in glioblastoma. Cancer Res 80:30–43. https://doi.org/10.1158/0008-5472.CAN-19-1389.

24. Hyde BB, Twig G, Shirihai OS. 2010. Organellar vs cellular control of mitochondrial dynamics. Semin Cell Dev Biol 21:575–581. https://doi.org/10.1016/j.semcdb.2010.01.003.

25. Park HJ, Jo DS, Choi DS, Bae J-E, Park NY, Kim J-B, Chang JH, Shin JJ, Cho D-H. 2020. Ursolic acid inhibits pigmentation by increasing melanosomal autophagy in B16F1 cells. Biochem Biophys Res Commun 531:209–214. https://doi.org/10.1016/j.bbrc.2020.07.125.

26. Dai Y, Cai Y, Wang X, Zhu J, Liu X, Liu H, Li L, Zhang Y, Liu S, Wen Z, Feng CG, Chen X, Tang X. 2020. Autoantibody-mediated erythrophagocytosis increases tuberculosis susceptibility in HIV patients. mBio 11:e03246-19. https://doi.org/10.1128/mBio.03246-19.

27. Ye X, Zhou XJ, Zhang H. 2018. Exploring the role of autophagy-related gene 5 (ATG5) yields important insights into autophagy in autoimmune/autoinflammatory diseases. Front Immunol 9:2334. https://doi.org/10.3389/fimmu.2018.02334.

28. Cahill C, Phelan JJ, Keane J. 2020. Understanding and exploiting the effect of tuberculosis antimicrobials on host mitochondrial function and bioenergetics. Front Cell Infect Microbiol 10:493. https://doi.org/10.3389/fcimb.2020.00493.

29. Vijayan V, Pradhan P, Braud L, Fuchs HR, Gueler F, Motterlini R, Foresti R, Immenschuh S. 2019. Human and murine macrophages exhibit differential metabolic responses to lipopolysaccharide - a divergent role for glycolysis. Redox Biol 22:101147. https://doi.org/10.1016/j.redox.2019.101147.

30. Chen M, Gan H, Remold HG. 2006. A mechanism of virulence: virulent Mycobacterium tuberculosis strain H37Rv, but not attenuated H37Ra, causes significant mitochondrial inner membrane disruption in macrophages leading to necrosis. J Immunol 176:3707–3716. https://doi.org/10.4049/jimmunol.176.6.3707.

31. Korchak HM, Rich AM, Wilkenfeld C, Rutherford LE, Weissmann G. 1982. A carbocyanine dye, DiOC6(3), acts as a mitochondrial probe in human neutrophils. Biochem Biophys Res Commun 108:1495–1501. https://doi.org/10.1016/s0006-291x(82)80076-4.

32. Terasaki M, Song J, Wong JR, Weiss MJ, Chen LB. 1984. Localization of endoplasmic reticulum in living and glutaraldehyde-fixed cells with fluorescent dyes. Cell 38:101–108. https://doi.org/10.1016/0092-8674(84)90530-0.

33. Sabnis RW, Deligeorgiev TG, Jachak MN, Dalvi TS. 1997. DiOC63: a useful dye for staining the endoplasmic reticulum. Biotech Histochem 72:253–258. https://doi.org/10.3109/10520299709082249.

34. Salvioli S, Ardizzoni A, Franceschi C, Cossarizza A. 1997. JC-1, but not DiOC6(3) or rhodamine 123, is a reliable fluorescent probe to assess ΔΨ changes in intact cells: implications for studies on mitochondrial functionality during apoptosis. FEBS Lett 411:77–82. https://doi.org/10.1016/s0014-5793(97)00669-8.

35. Xu F, Qi H, Li J, Sun L, Gong J, Chen Y, Shen A, Li W. 2020. Mycobacterium tuberculosis infection upregulates MFN2 expression to promote NLRP3 inflammasome formation. J Biol Chem 295:17684–17697. https://doi.org/10.1074/jbc.RA120.014077.

36. Tur J, Pereira-Lopes S, Vico T, Marin EA, Munoz JP, Hernandez-Alvarez M, Cardona PJ, Zorzano A, Lloberas J, Celada A. 2020. Mitofusin 2 in macrophages links mitochondrial ROS production, cytokine release, phagocytosis, autophagy, and bactericidal activity. Cell Rep 32:108079. https://doi.org/10.1016/j.celrep.2020.108079.

37. Lloberas J, Munoz JP, Hernandez-Alvarez MI, Cardona PJ, Zorzano A, Celada A. 2020. Macrophage mitochondrial MFN2 (mitofusin 2) links immune stress and immune response through reactive oxygen species (ROS) production. Autophagy 16:2307–2309. https://doi.org/10.1080/15548627.2020.1839191.

38. Zhang Z, Li TE, Chen M, Xu D, Zhu Y, Hu BY, Lin ZF, Pan JJ, Wang X, Wu C, Zheng Y, Lu L, Jia HL, Gao S, Dong QZ, Qin LX. 2020. MFN1-dependent alteration of mitochondrial dynamics drives hepatocellular carcinoma metastasis by glucose metabolic reprogramming. Br J Cancer 122:209–220. https://doi.org/10.1038/s41416-019-0658-4.

39. Noguchi M, Hirata N, Tanaka T, Suizu F, Nakajima H, Chiorini JA. 2020. Autophagy as a modulator of cell death machinery. Cell Death Dis 11:517. https://doi.org/10.1038/s41419-020-2724-5.

40. Li FJ, Xu ZS, Soo AD, Lun ZR, He CY. 2017. ATP-driven and AMPK-independent autophagy in an early branching eukaryotic parasite. Autophagy 13:715–729. https://doi.org/10.1080/15548627.2017.1280218.

41. Schellens JP, Vreeling-Sindelárová H, Plomp PJ, Meijer AJ. 1988. Hepatic autophagy and intracellular ATP. A morphometric study. Exp Cell Res 177:103–108. https://doi.org/10.1016/0014-4827(88)90028-6.

42. Cogliati S, Frezza C, Soriano ME, Varanita T, Quintana-Cabrera R, Corrado M, Cipolat S, Costa V, Casarin A, Gomes LC, Perales-Clemente E, Salviati L, Fernandez-Silva P, Enriquez JA, Scorrano L. 2013. Mitochondrial cristae shape determines respiratory chain supercomplexes assembly and respiratory efficiency. Cell 155:160–171. https://doi.org/10.1016/j.cell.2013.08.032.

43. Tondera D, Grandemange S, Jourdain A, Karbowski M, Mattenberger Y, Herzig S, Da Cruz S, Clerc P, Raschke I, Merkwirth C, Ehses S, Krause F, Chan DC, Alexander C, Bauer C, Youle R, Langer T, Martinou JC. 2009. SLP-2 is required for stress-induced mitochondrial hyperfusion. EMBO J 28:1589–1600. https://doi.org/10.1038/emboj.2009.89.

44. Amini P, Stojkov D, Felser A, Jackson CB, Courage C, Schaller A, Gelman L, Soriano ME, Nuoffer JM, Scorrano L, Benarafa C, Yousefi S, Simon HU. 2018. Neutrophil extracellular trap formation requires OPA1-dependent glycolytic ATP production. Nat Commun 9:2958. https://doi.org/10.1038/s41467-018-05387-y.

45. Tait SW, Green DR. 2012. Mitochondria and cell signalling. J Cell Sci 125:807–815. https://doi.org/10.1242/jcs.099234.

46. Dagda RK, Cherra SJ, 3rd, Kulich SM, Tandon A, Park D, Chu CT. 2009. Loss of PINK1 function promotes mitophagy through effects on oxidative stress and mitochondrial fission. J Biol Chem 284:13843–13855. https://doi.org/10.1074/jbc.M808515200.